International Journal of
Environmental Research and Public Health

MDPI

Article

Degradation Mechanisms of 4,7-Dihydroxycoumarin Derivatives in Advanced Oxidation Processes: Experimental and Kinetic DFT Study

Žiko Milanović [1], Dušan Dimić [2,*], Erik Klein [3], Monika Biela [3], Vladimír Lukeš [3], Milan Žižić [4], Edina Avdović [1], Drago Bešlo [5], Radiša Vojinović [6], Jasmina Dimitrić Marković [2] and Zoran Marković [1,7,*]

1 Department of Science, Institute for Information Technologies, University of Kragujevac, Jovana Cvijića bb, 34000 Kragujevac, Serbia
2 Faculty of Physical Chemistry, University of Belgrade, 12−16 Studentski Trg, 11000 Belgrade, Serbia
3 Institute of Physical Chemistry and Chemical Physics, Slovak University of Technology in Bratislava, Radlinského 9, SK-812 37 Bratislava, Slovakia
4 Life Sciences Department, Institute for Multidisciplinary Research, University of Belgrade, Kneza Višeslava 1, 11030 Belgrade, Serbia
5 Department of Agroecology and Environmental Protection, Faculty of Agrobiotechnical Sciences Osijek, University Josip Juraj Strossmayer Osijek, Vladimir Prelog 1, 31000 Osijek, Croatia
6 Faculty of Medical Sciences, University of Kragujevac, Svetozara Markovića 69, 34000 Kragujevc, Serbia
7 Department of Chemical-Technological Sciences, State University of Novi Pazar, Vuka Karadžića bb, 36300 Novi Pazar, Serbia
* Correspondence: ddimic@ffh.bg.ac.rs (D.D.); zmarkovic@uni.kg.ac.rs (Z.M.); Tel.: +381-34-610-01-95 (Z.M.)

Abstract: Coumarins represent a broad class of compounds with pronounced pharmacological properties and therapeutic potential. The pursuit of the commercialization of these compounds requires the establishment of controlled and highly efficient degradation processes, such as advanced oxidation processes (AOPs). Application of this methodology necessitates a comprehensive understanding of the degradation mechanisms of these compounds. For this reason, possible reaction routes between HO$^\bullet$ and recently synthesized aminophenol 4,7-dihydroxycoumarin derivatives, as model systems, were examined using electron paramagnetic resonance (EPR) spectroscopy and a quantum mechanical approach (a QM-ORSA methodology) based on density functional theory (DFT). The EPR results indicated that all compounds had significantly reduced amounts of HO$^\bullet$ radicals present in the reaction system under physiological conditions. The kinetic DFT study showed that all investigated compounds reacted with HO$^\bullet$ via HAT/PCET and SPLET mechanisms. The estimated overall rate constants ($k_{overall}$) correlated with the EPR results satisfactorily. Unlike HO$^\bullet$ radicals, the newly formed radicals did not show (or showed negligible) activity towards biomolecule models representing biological targets. Inactivation of the formed radical species through the synergistic action of O_2/NO_x or the subsequent reaction with HO$^\bullet$ was thermodynamically favored. The ecotoxicity assessment of the starting compounds and oxidation products, formed in multistage reactions with O_2/NO_x and HO$^\bullet$, indicated that the formed products showed lower acute and chronic toxicity effects on aquatic organisms than the starting compounds, which is a prerequisite for the application of AOPs procedures in the degradation of compounds.

Keywords: 4,7-dihydroxycoumarin; DFT; EPR; AOPs; radical scavenging; hydroxyl radical; QM−ORSA

Citation: Milanović, Ž.; Dimić, D.; Klein, E.; Biela, M.; Lukeš, V.; Žižić, M.; Avdović, E.; Bešlo, D.; Vojinović, R.; Dimitrić Marković, J.; et al. Degradation Mechanisms of 4,7-Dihydroxycoumarin Derivatives in Advanced Oxidation Processes: Experimental and Kinetic DFT Study. *Int. J. Environ. Res. Public Health* **2023**, *20*, 2046. https://doi.org/10.3390/ijerph20032046

Academic Editor: Paul B. Tchounwou

Received: 9 December 2022
Revised: 15 January 2023
Accepted: 19 January 2023
Published: 22 January 2023

1. Introduction

The rapid advancement of synthetic organic chemistry has led to the appearance of numerous compounds with remarkable biological properties. Available literature data indicate that various newly synthesized coumarin derivatives have pronounced pharmacological and biological properties, such as anticarcinogenic [1,2], antimicrobial [3,4],

antioxidant [5,6], antiviral [7,8], and, especially, anticoagulant activities [9,10]. Coumarin derivatives, such as warfarin and coumatetralyl, are some of the most frequently used anticoagulant agents [11]. On the other hand, the mentioned compounds are also potent rodenticides that act through the same anticoagulant mechanism [12]. Due to their pharmaceutical and industrial applications, significant concentrations of these compounds and their hydroxylated derivatives are present in wastewater treatment plants, from where they often end up in natural receiving waters as part of effluents [13,14]. Due to their stability and persistence, coumarin derivatives reabsorbed in the diets of aquatic organisms can be especially dangerous. Their pronounced biological activity and the potential application of newly synthesized coumarin derivatives in industry have resulted in the need for a specific, highly efficient methodology for the study of their degradation. In recent decades, particular emphasis has been placed on the application of techniques based on advanced oxidation processes (AOPs) [15,16]. The first step in AOPs is the in situ generation of strong oxidants—e.g., through the Fenton reaction or photocatalytic oxidation—capable of oxidizing various compounds [17,18]. However, the application of this methodology requires the development of a strategy and modeling of the reaction process. This necessitates a comprehensive investigation of the mechanisms of the reaction between the highly reactive radical species and the corresponding compound, as well as an assessment of the toxicity of the formed intermediates [19]. Reliable knowledge about the possible mechanisms, intermediates, and final products is crucial for successful modeling of AOPs. Standard experimental techniques are often limited in providing unambiguous identification of mechanisms due to the formation of unstable intermediates that are difficult to detect [20].

For this reason, the degradation mechanisms of previously synthesized aminophenol 4,7-dihydroxycoumarin derivatives (Figure 1) [21] were examined in this study under AOP conditions ($HO^{\bullet}$) as examples of stable aromatic compounds utilizing the sophisticated Electron paramagnetic resonance (EPR) spectroscopy experimental technique and a theoretical quantum mechanics-based test for overall radical scavenging activity (the QM-ORSA methodology) [22] based on density functional theory (DFT). The structure of these compounds offers the possibility of analyzing the effect of the substituent (–OH) position on the reaction parameters. A similar methodology has been successfully applied to other coumarin derivatives [23,24].

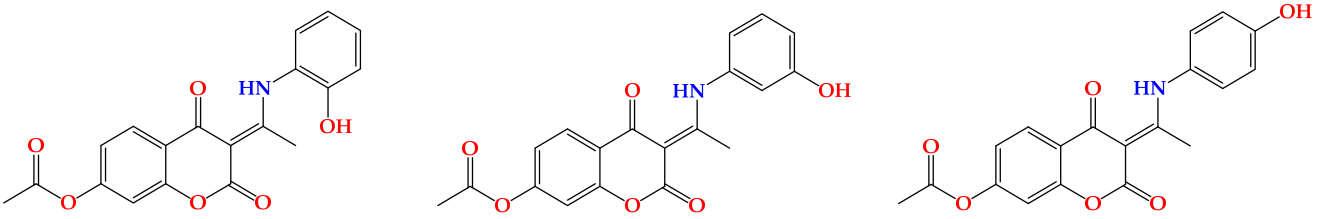

Figure 1. Structures of previously synthesized [21] aminophenol derivatives of 4,7−dihydroxycoumarin.

The applied methodology was based on the calculation of the thermodynamic and kinetic parameters of generally accepted radical scavenging mechanisms, such as hydrogen atom transfer (HAT), single-electron transfer followed by proton transfer (SE−TPT), sequential proton loss followed by electron transfer (SPLET), and radical adduct formation (RAF) [25,26]. In addition, assessment of the reactivity of the newly formed radical species utilizing appropriate models for biomolecular targets was one of the main goals of this work, since one of the prerequisites for AOPs is the lower reactivity of final products. A theoretical prediction of the ecotoxicity of the formed products toward aquatic organisms was also calculated using available software resources. The obtained results for the title compounds, as model systems, represent a basis for future investigations into the degradation processes of different coumarin derivatives.

2. Materials and Methods

2.1. Chemicals and Instrumentations

Chemicals used in the synthesis and spectroscopic EPR measurements were obtained from Merck (Darmstadt, Germany), except for spin-trap DEPMPO, which was purchased from Enzo Life Sciences (Farmingdale, NY, USA).

2.2. EPR Measurement with HO• Radical

The Bruker EMX Nano X-band (9.65 GHz) spectrometer was used for the EPR measurements, which were conducted at room temperature (293 K) using the following experimental parameters: 10 dB power attenuation; 2 mT modulation amplitude; 100 kHz modulation frequency; and 120 s sweep time. The hydroxyl radical (HO•) was generated in 100 mM phosphate buffer, pH = 7.4, using the standard Fenton reaction (1 mM H_2O_2 and 0.33 mM $FeSO_4$) with the addition of 0.1 M 2-diethoxyphosphoryl-2-methyl-1-oxido-3,4-dihydropyrrol-1-ium (DEPMPO) as a spin-trapping agent. Spectra collection started 180 s after the addition of the iron catalyst. Jackson's procedure for purifying the spin trap was followed [27]. Stock solutions of compounds (15 mM) were prepared in DMSO and diluted to 10 µM with water. The amount of DMSO in the blank sample was the same as in the samples containing the investigated compounds. The final concentration of the examined compounds was 0.75 µM. The average intensity of the two most intense peaks of the DEPMPO–HO• adduct at the low-field region of the spectrum was used to calculate reactivities to HO•. Measurement results are expressed as the % of radical reduction = 100 $\times$ $(I_0 - I_a)/I_0$. In the previous equation, I_a and I_0 are the intensities of the peaks of the DEPMPO–HO• adduct with and without the investigated compounds (A_1–RH–A_3–RH), respectively.

2.3. Computational Methodology

The Gaussian09 program package [28] was used for all the calculations based on density functional theory (DFT). The M06-2X/6-311++G(d,p) theoretical model (with polarization and diffuse functions included) was employed for the optimization of the structures of the coumarin derivatives, as suggested in [29]. The applied theoretical model is suitable for thermodynamic and kinetic analyses of various reactions [23–25,30,31]. The conductor-like polarizable continuum model (CPCM, water (ε = 78.36)) was applied to approximate the solvent effect in the experimental environment [32].

The radical mechanisms presented in this study were evaluated based on thermodynamic and kinetic considerations. This was consistent with the quantum mechanics-based test for overall free radical scavenging activity (QM-ORSA) methodology [22], commonly used to determine antiradical activity. After the calculation of the corresponding reaction Gibbs free energies ($\Delta_r G$), kinetic calculations were performed for all exergonic ($\Delta_r G < 0$) and isoergonic ($\Delta_r G = 0$) reaction pathways. The rate constants (k) were calculated using transition state theory (TST) [33] or the Eyring equation, as well as Eckart's method, which represents the special case of the zero-curvature tunneling approach (ZCT_0) [34]. The first theory is based on the laws of classical kinetics, whereas the second includes quantum effects, such as tunneling (Equation (1)):

$$k_{ZCT\_0} = \sigma\gamma(T)\frac{k_B T}{h}\exp\left(\frac{-\Delta G_a^{\neq}}{RT}\right) \quad (1)$$

where k_B and h are the Boltzmann and Planck constants; T is the temperature in K (298.15 K); $\Delta G_a^{\neq}$ is the activation Gibbs free energy; σ represents the reaction path degeneracy accounting for the number of equivalent reaction paths; and $\gamma(T)$ is the tunneling correction [35]. For these calculations, *TheRate* program was used [36].

Evaluation of the overall rate constant ($k_{overall}$) in a polar medium offers a comprehensive picture of the reactivity of the investigated compounds. The $k_{overall}$ is the sum of the products of the molar fractions of acid–base species included in specific reactions and

the total rate constant (k_{tot}). The k_{tot} comprises the sum of all kinetically favored reaction pathways for a particular species. A detailed explanation of the $k_{overall}$ estimation, the process of quantifying molar fractions of acid–base species at physiological pH, is given in previous research [23]. Additionally, the equations for the estimation of reactivity towards a specific radical (r^T) relative to the reference standard antioxidant (Trolox), as well as relative amounts of products (%)—i.e., the branching ratios (Γ_i)—are integral parts of a previous report [23].

The Ecological Structure–Activity Relationships program (ECOSAR V2.0) [37] was used to evaluate the acute and chronic toxicities (ChV, $mg \cdot L^{-1}$) of the investigated compounds and their oxidation products towards aquatic organisms: green algae, fish, and daphnia. Acute toxicity was defined using EC_{50} values (the concentration of the examined compound that affected the growth of 50% of green algae after 96 h of exposure) and LC_{50} values (the concentration of the investigated compound that caused 50% mortality in fish and daphnia after 96 h) [38,39].

The estimated $k_{overall}$ values made it possible to determine the stability of the investigated compounds during their degradation initiated by $HO^{\bullet}$ radicals through the half-life ($\tau_{1/2}$) using the following equation:

$$\tau_{1/2} = \ln 2 / k_{overall} \times [HO^{\bullet}] \quad (2)$$

where $[HO^{\bullet}]_{aq}$ is the concentration of $HO^{\bullet}$ in an aqueous solution [40].

To examine the activity of the newly formed radical products ($\mathbf{A_1–R^{\bullet}}$, $\mathbf{A_2–R^{\bullet}}$, $\mathbf{A_3–R^{\bullet}}$) towards biologically essential macromolecules, interactions with three groups of building blocks were considered: model lipids, amino acid residues, and nucleobases, as depicted in Figure 2 [41]. The lipid model (LM) mimics unsaturated fatty acids as essential biomolecules. It is represented as a reduced linoleic acid (LA) model that retains its primary chemical reactivity characteristic: two allylic H atoms. Amino acids, as constituents of proteins, are modeled realistically. This model has been successfully used and is widely accepted as appropriate for investigating protein site reactions. The following residues, being the most susceptible to oxidative damage in proteins, were used in this study: cysteine (Cys), leucine (Leu), tyrosine (Tyr), tryptophan (Trp), methionine (Met), and histidine (His). 2′-Deoxyguanosine (2dG) was selected as a model for oxidative DNA damage because guanine (G) is the most easily oxidized nucleobase. Therefore, when one-electron oxidation of DNA occurs, it is primarily located at G sites. Consequently, if a chemical oxidant (radical species) can oxidize 2dG, it can cause oxidative damage to DNA. In contrast, if there is no potential to oxidize 2dG, the oxidant is considered harmless to DNA.

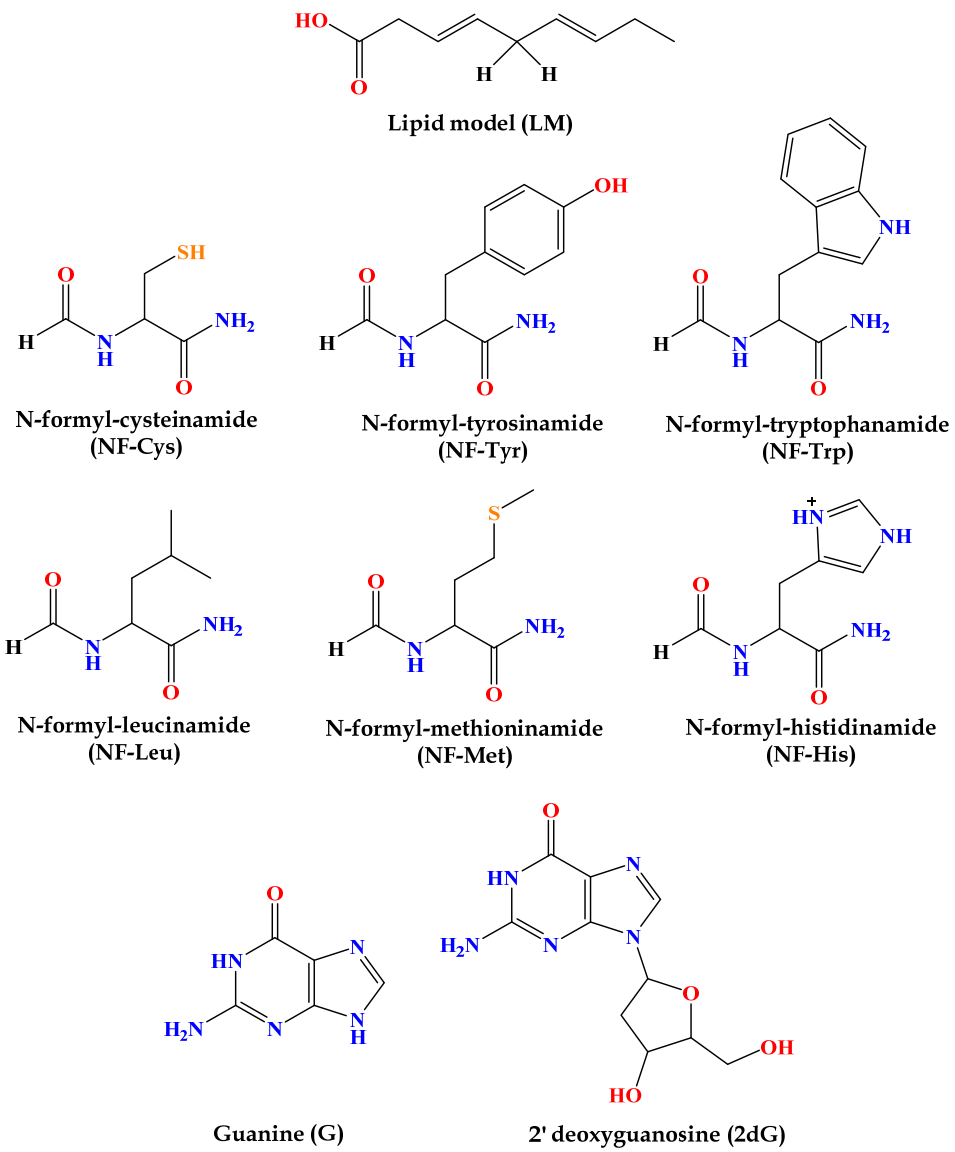

Figure 2. Structures of investigated molecular targets—constituents of important molecules: phospholipid bilayer, proteins, and nucleic acids.

3. Results and Discussion

3.1. Experimental HO• Scavenging Activity

EPR spectroscopy was used to trace the reactivity of the obtained compounds toward HO•. All spectra were collected starting from the same time point—180 s after the reaction beginning. Scavenged HO• radicals were formed in the Fenton system, and DEPMPO was used as a spin trap to enable the monitoring of the decrease in the HO• concentration. Figure 3 shows the EPR spectra of DEPMPO–HO• adducts before and after the addition of A_1–RH to A_3–RH compounds. Signal intensity, proportional to the number of scavenged radical species, was reduced after addition of coumarin derivatives, indicating the reaction between the investigated compounds and HO•. The reactivity of the investigated compounds towards HO• was calculated as explained in the Materials and Methods section. The scavenging activities decreased in the following order: A_1–RH (91%) > A_2–RH (88%) > A_3–RH (81%). Differences in these values indicate the variation in the reactivity of the investigated compounds. The studied coumarin derivatives contained the –OH group in various positions relative to the –NH– group and the rest of the molecule, leading to different reactivities. This group made hydrogen atom/proton abstraction possible in the standard

examination of the activity towards radicals. The amino group was not considered a potential hydrogen atom/proton donor, as this hydrogen atom encloses a quasi-six-membered ring through a hydrogen bond with the carbonyl group, as previously observed in the crystal structure of similar compounds [42–44]. The most reactive compound was A_1–RH, which can be explained by the possible formation of hydrogen bonds between oxygen and the NH group upon the reaction with $HO^{\bullet}$. Due to the existence of a negative charge in the aromatic ring, higher reactivity for A_3–RH was expected in comparison to A_2–RH. Radical adduct formation (RAF) is another plausible mechanism, as these compounds contain many unsaturated bonds [45,46]. The following sections include a detailed quantum chemical analysis of the oxidation process, emphasizing the role of acid-base equilibria. Hydrogen atom transfer (HAT), the direct exchange of protons followed by the transfer of electrons from formed anions, and the formation of radical adducts are the most probable reaction pathways for coumarin derivatives [23,24]. These mechanisms play crucial roles in the synergy between the elimination of radical species from wastewater and the production of less harmful oxidation products [47–50].

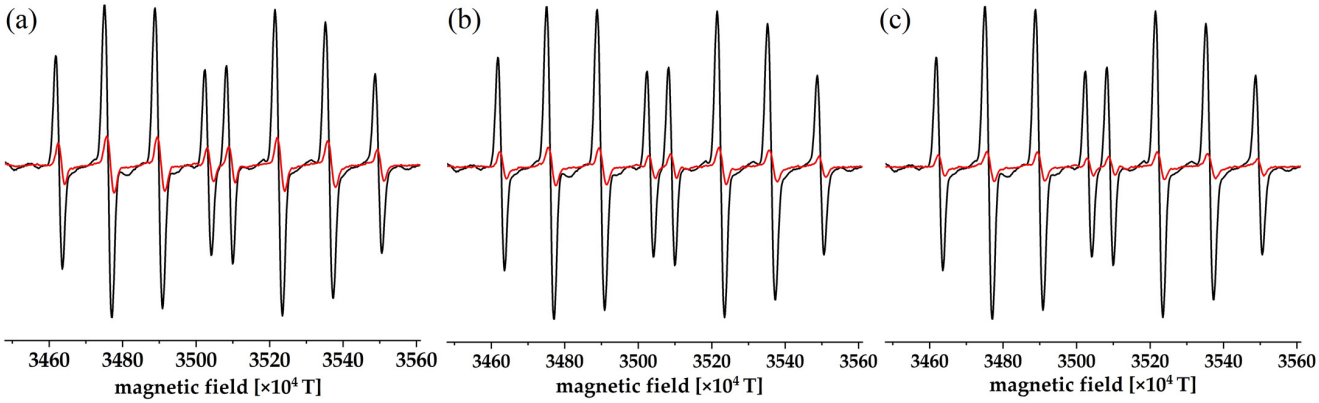

Figure 3. The experimental EPR spectra of DEPMPO−$HO^{\bullet}$ in the presence (red line) and absence (black line) of the compounds (**a**) A_1–RH, (**b**) A_2–RH, and (**c**) A_3–RH.

3.2. Acid-Base Equilibria

As the acid–base equilibrium determines the relative abundance of protonated/deprotonated forms present in an aqueous solution, it is evident that the pH value of the solution determines the dominant mechanism of free radical scavenging. The degree of deprotonation of a compound, expressed through the corresponding *p*Ka value, determines various physicochemical properties, such as hydrophobicity, lipophilicity, polarizability, etc. Quantifying the molar fractions of acid–base species provides a comprehensive way of examining the mechanisms of radical scavenging action. Therefore, it was necessary to determine the *p*Ka values to obtain the deprotonation route and quantify the molar fractions (*f*). The ACD/pK_a software package was employed to calculate the pK_a values of studied derivatives [51]. Figure 4 shows their deprotonation routes, as well as the estimated *p*Ka values and molar fraction (*f*) values under physiological conditions. The pK_a values depend on the position of the –OH group. As there were no additional stabilization effects in the formed anion, the *meta*-substituted derivative (**A_2–R^-**) showed the lowest value (pK_a = 9.64). The **A_1–R^-** anion (pK_a = 9.71) was stabilized by the intramolecular hydrogen bond between the amino group and the oxygen atom. The extended delocalization in the aromatic ring of the formed anion **A_3–R^-** was responsible for the highest pK_a value (pK_a = 10.43). This analysis proves that hydrogen atom/proton donation is only possible from the –OH group.

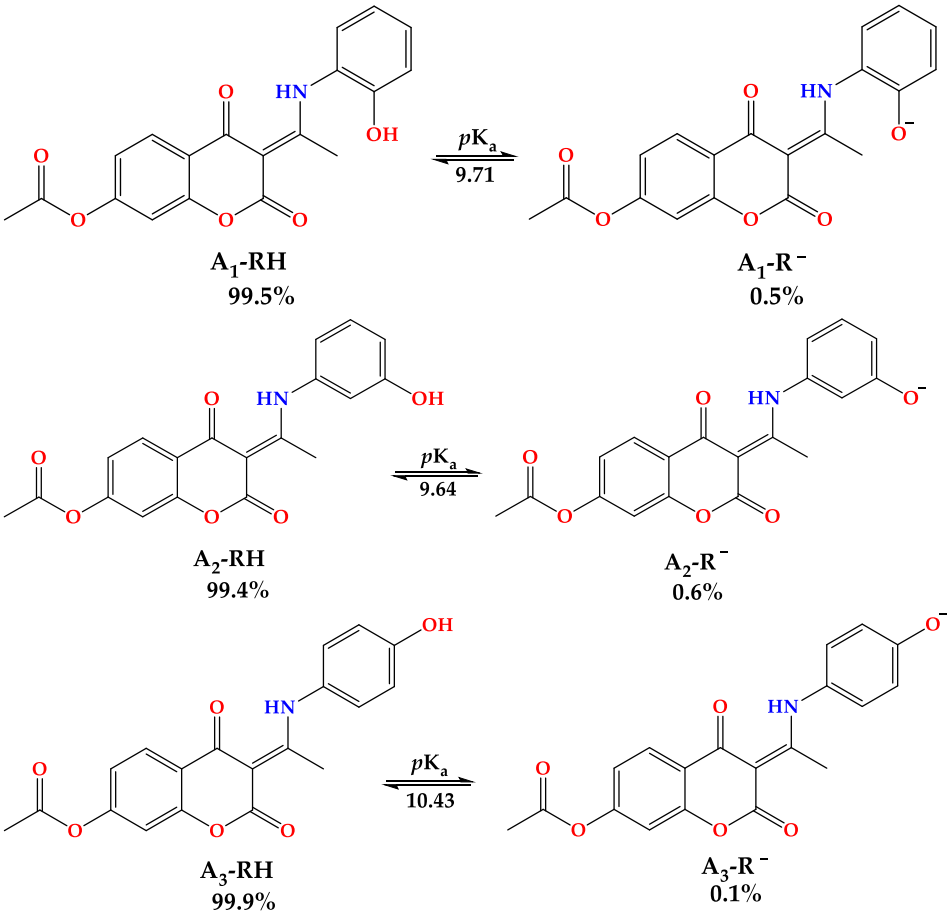

Figure 4. Deprotonation process, estimated pK_a values, and molar fractions (f) of acid–base species of newly synthesized aminophenol derivatives of 4,7−dihydroxycoumarin (A_1RH to A_3RH) at physiological pH = 7.4.

Based on the obtained pK_a values, neutral species dominate (>99%) at physiological pH. Due to this fact, theoretical investigations were performed on neutral forms: A_1–RH (99.5%), A_2–RH (99.4%), and A_3–RH (99.9%). Their optimized structures, with carbon atom numbering schemes, are shown in Figure 5.

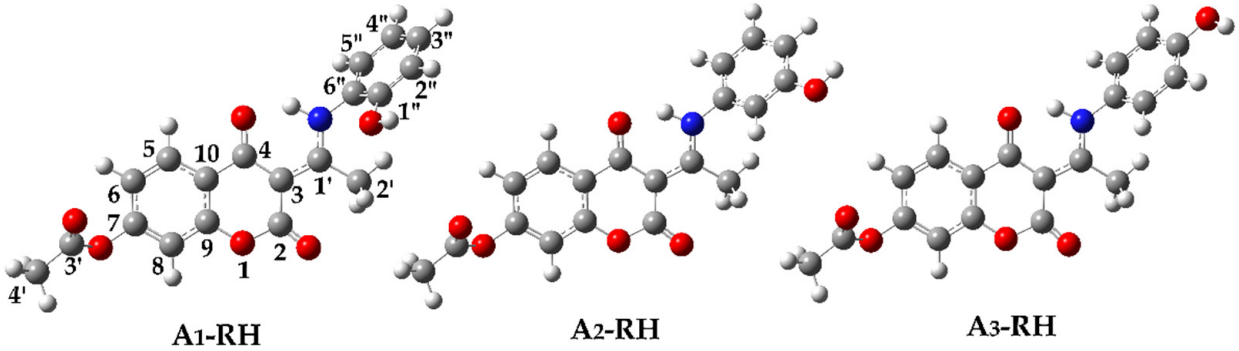

Figure 5. Optimized geometries of investigated compounds in water at M06-2X/6-311++G(d,p) level of theory with carbon atom numbering scheme.

3.3. Reactions of A_n–RH with HO• Radical—Thermodynamic Approach

The possible reaction centers for the standard mechanisms (HAT/PCET (Equation (3)), SPLET (Equations (4) and (5)), and SETPT (Equations (6) and (7))) of radical action between A_1–RH, A_2–RH, A_3–RH, and HO• were aromatic –OH groups. For the RAF mechanism,

these centers included aromatic carbon atoms (Equation (8)). The calculated values of the reaction Gibbs energies ($\Delta_r G$) for the mentioned mechanisms are listed in Table 1.

$$\text{HAT: } A_n\text{-RH} + HO^{\bullet} \rightarrow A_n\text{-R}^{\bullet} + H_2O \quad (3)$$

$$\text{SPL: } A_n\text{-RH} + HO^{-} \rightarrow A_n\text{-R}^{-} + H_2O \quad (4)$$

$$\text{ET: } A_n\text{-R}^{-} + HO^{\bullet} \rightarrow A_n\text{-R}^{\bullet} + HO^{-} \quad (5)$$

$$\text{SET: } A_n\text{-RH} + HO^{\bullet} \rightarrow A_n\text{-RH}^{\bullet+} + HO^{-} \quad (6)$$

$$\text{PT: } A_n\text{-RH}^{\bullet+} + HO^{-} \rightarrow A_n\text{-R}^{\bullet} + H_2O \quad (7)$$

$$\text{RAF: } A_n\text{-RH} + HO^{\bullet} \rightarrow [\text{HO-}A_n\text{-RH}]^{\bullet} \quad (8)$$

Table 1. Estimated values of reaction Gibbs energies ($\Delta_r G$) in kJ·mol^{-1} for reactions between coumarin derivatives (A_1–RH, A_2–RH, A_3–RH) and $HO^{\bullet}$ at 298.15 K.

Species	**$HO^{\bullet}$**				
	HAT/PCET	**SET−PT**		**SPLET**	
	$\Delta_r G_{HAT/PCET}$	**$\Delta_r G_{SET}$**	**$\Delta_r G_{PT}$**	**$\Delta_r G_{SPL}$**	**$\Delta_r G_{ET}$**
A_1–RH	−127	139	−266	−115	−13
A_2–RH	−124	144	−268	−103	−21
A_3–RH	−126	122	−248	−115	−28
Positions	**RAF, $\Delta_r G_{RAF}$**				
	A_1–RH	**A_2–RH**	**A_3–RH**		
C3	−7	−15	−5		
C5	−41	−43	−37		
C6	−18	−21	−17		
C7	−44	−43	−40		
C8	−34	−36	−35		
C9	−31	−35	−29		
C10	2	−4	4		
C1′	−27	−27	−24		
C1″	−35	−27	−34		
C2″	−43	−38	−17		
C3″	−30	−34	−31		
C4″	−22	−42	−40		
C5″	−24	−22	−32		
C6″	−31	−21	−30		

According to the $\Delta_r G$ values shown in Table 1 for the first step of each mechanism, HAT/PCET was thermodynamically favored for all derivatives. The reactivity of the compounds and the stability of the formed radical products increased in the following order: A_2–RH (−124 kJ·mol^{-1}) > A_3–RH (−126 kJ·mol^{-1}) > A_1–RH (−127 kJ·mol^{-1}). This order nicely follows the discussion on the possible stabilization effects of proton removal in acid-base equilibrium processes.

Negative $\Delta_r G_{RAF}$ values made the RAF mechanism thermodynamically spontaneous in almost all the positions of the investigated compounds. The most favored positions for attack by electrophilic $HO^{\bullet}$ were the C5 (from −43 to −37 kJ·mol^{-1}) and C7 (from −44 to −40 kJ·mol^{-1}) atoms of the aromatic part of the chroman ring, as well as the C1″ to C6″ positions of the aromatic aminophenol rings. As mentioned, the aromatic carbon atoms of both rings were possible reaction sites. It is essential to notice that the values for the chroman part of the molecule did not significantly depend on the position of the substituent (around 5 kJ·mol^{-1} difference), with the exception of position C3. When aminophenol carbon atoms were involved, noticeable differences were only obtained for the carbon atoms adjacent to the position of the –OH group. However, slightly endergonic values for the C10

position of the A_1–RH (2 kJ·mol^{-1}) and A_3–RH (4 kJ·mol^{-1}) compounds were obtained. In the optimized geometries of radical adducts (Figures S1–S3), the rehybridization of the carbon atom (sp^2 to sp^3) where the HO$^\bullet$ radical was attached occurred, leading to broken aromaticity and planarity in the system. The most thermodynamically favored products were characterized by short interatomic distances in adducts C−2″ (A_1–RH, 1.408 Å), C−3″ (A_2–RH, 1.405 Å), and C−5″ (A_3–RH, 1.405 Å) due to stabilization by intramolecular contacts (Figures S1–S3).

For all the examined compounds, significantly negative $\Delta_r G_{SPL}$ values indicated that the first step of the SPLET mechanism was thermodynamically spontaneous (Table 1). The reactivity of the compounds and the stability of the formed anionic species increased in the following sequence: A_2–RH (−103 kJ·mol^{-1}) > A_1–RH (−115 kJ·mol^{-1}) ≥ A_3–RH (−115 kJ·mol^{-1}), with the same plausible explanation as for the first mechanism. Comparison of $\Delta_r G_{HAT/PCET}$ and $\Delta_r G_{SPL}$ indicated that the hydrogen atom transfer from the –OH group was slightly more favored than the proton transfer. In the second step of the SPLET mechanism—i.e., electron transfer—$\Delta_r G_{ET}$ values decreased in the following sequence: A_1–RH (−13 kJ·mol^{-1}) > A_2–RH (−21 kJ·mol^{-1}) > A_3–RH (−28 kJ·mol^{-1}). These values depended on the spin delocalizations in the formed radicals.

Finally, highly endergonic values (122–144 kJ·mol^{-1}) for the first step of the SET−PT mechanism ($\Delta_r G_{SET}$) suggested that this mechanism was not thermodynamically probable. Thus, it was not considered in further kinetic studies (Table 1).

3.4. Reactions of A_n–RH with HO$^\bullet$ Radical—Kinetic Approach

Thermodynamically favored reaction pathways ($\Delta_r G \leq 0$) were subjected to kinetic investigation. After locating the transition state geometries (where possible), the activation Gibbs energies (ΔG_a) were evaluated. Rate constants for reactions involving electron transfer were calculated using Marcus theory (Table 2). The rate constants were estimated using the TST (Table S1) and ZCT_0 (Table 2) methods.

Table 2. Estimated values of kinetic parameters at 298.15 K: activation Gibbs energy (ΔG_a, kJ·mol^{-1}) and rate constants of the bimolecular chemical reactions (M^{-1} s^{-1}) between the investigated compounds A_1–RH, A_2–RH, and A_3–RH and HO$^\bullet$ estimated with the Eckart method (k_{ZCT_0}). The k^{ET} values (M^{-1} s^{-1}) represent rate constants calculated with Marcus theory.

Species	HAT/PCET		SPLET			
	$\Delta G_a^{HAT/PCET}$	$k_{ZCT\_0}^{HAT/PCET}$	ΔG_a^{SPL}	k^{SPL}	ΔG_a^{ET}	k^{ET}
A_1–RH					2	8.02×10^9
A_2–RH	~0	1.91×10^9	~0	1.91×10^9	2	8.01×10^9
A_3–RH					6	7.90×10^9
Position	**A_1–RH**		**A_2–RH**		**A_3–RH**	
	ΔG_a^{RAF}	$k_{ZCT\_0}^{RAF}$	ΔG_a^{RAF}	$k_{ZCT\_0}^{RAF}$	ΔG_a^{RAF}	$k_{ZCT\_0}^{RAF}$
C3	40	1.61×10^7	41	1.48×10^7	47	1.22×10^6
C5	54	7.15×10^4	51	2.77×10^5	53	1.11×10^5
C6	56	3.34×10^4	53	1.35×10^5	55	4.66×10^4
C7	60	7.54×10^3	51	2.80×10^5	63	2.31×10^3
C8	47	1.33×10^6	44	3.46×10^6	53	1.19×10^5
C9	56	3.12×10^4	53	1.35×10^5	57	2.12×10^4
C10	50	4.15×10^5	46	1.85×10^6	52	1.49×10^5
C1′	54	8.03×10^4	50	3.72×10^5	55	4.55×10^4
C1″	41	1.29×10^7	51	2.53×10^5	41	1.34×10^7
C2″	47	1.35×10^6	36	4.46×10^7	49	5.96×10^5
C3″	41	1.20×10^7	48	1.48×10^7	39	2.44×10^7
C4″	48	7.15×10^5	33	1.39×10^8	52	1.46×10^5
C5″	42	7.94×10^6	51	2.78×10^5	39	2.55×10^7
C6″	42	3.34×10^6	32	5.66×10^7	43	5.55×10^6

The pronounced exergonic values for hydrogen atom transfer (HAT/PCET) between A_n–RH and HO$^\bullet$ indicate the thermodynamic favorability of this mechanism. However, attempts to find transition state geometries describing these reactions have been unsuccessful. Thus, it is reasonable to assume that these reactions occur in a practically barrier-less manner [25]. To confirm the above assumption, the energy change as a function of the corresponding distance—i.e., HO–H2″ (−OH, Å) (A_1–RH), HO–H3″ (−OH, Å) (A_2–RH), HO–H4″ (−OH, Å) (A_3–RH)—was monitored (Figure S4). Analyzing Figure S4, it was discovered that there was a constant decrease in total energy as a function of distance from −1314.79 to −1314.87 a.u. This means that the reaction takes place without an activation barrier as a diffusion-controlled process with the rate constant, based on available literature data, of 1.91×10^9 $M^{-1} \cdot s^{-1}$ [52–54].

Another plausible mechanistic pathway for the reaction of HO$^\bullet$ with the investigated compounds is the RAF mechanism. The values of the rate constants estimated with the ZCT_0 method (Table 2) correlate with the values estimated with the TST method (Table S1). The rate constants obtained were in the range of 10^3 to 10^7 $M^{-1} \cdot s^{-1}$. Comparison of thermodynamic and kinetic parameters provided evidence that thermodynamically favored products are not necessarily kinetically preferred. The kinetically most preferred positions for HO$^\bullet$ attack were C1″ (1.29×10^7 $M^{-1} \cdot s^{-1}$) and C3″ (1.20×10^7 $M^{-1} \cdot s^{-1}$) for A_1–RH, C2″ (4.46×10^7 $M^{-1} \cdot s^{-1}$) and C4″ (1.39×10^8 $M^{-1} \cdot s^{-1}$) for A_2–RH, and C3″ (2.44×10^7 $M^{-1} \cdot s^{-1}$) and C5″ (2.55×10^7 $M^{-1} \cdot s^{-1}$) for A_3–RH, with ΔG_a values in the interval from 36 to 41 kJ·mol^{-1}. The optimized geometries of the corresponding transition states are shown in Figure 6, Figures S5 and S6. The transition states of the kinetically most favored products were characterized by larger interatomic distances: C1″ (2.047 Å) and C3″ (2.070 Å) for A_1–RH, C2″ (2.093 Å) and C4″ (2.115 Å) for A_2–RH, and C3″ (2.077 Å) and C5″ (2.088 Å) for A_3–RH. Moreover, the geometries of the mentioned transition states were stabilized by hydrogen bonds between the reactive HO$^\bullet$ particle and the polar functional group.

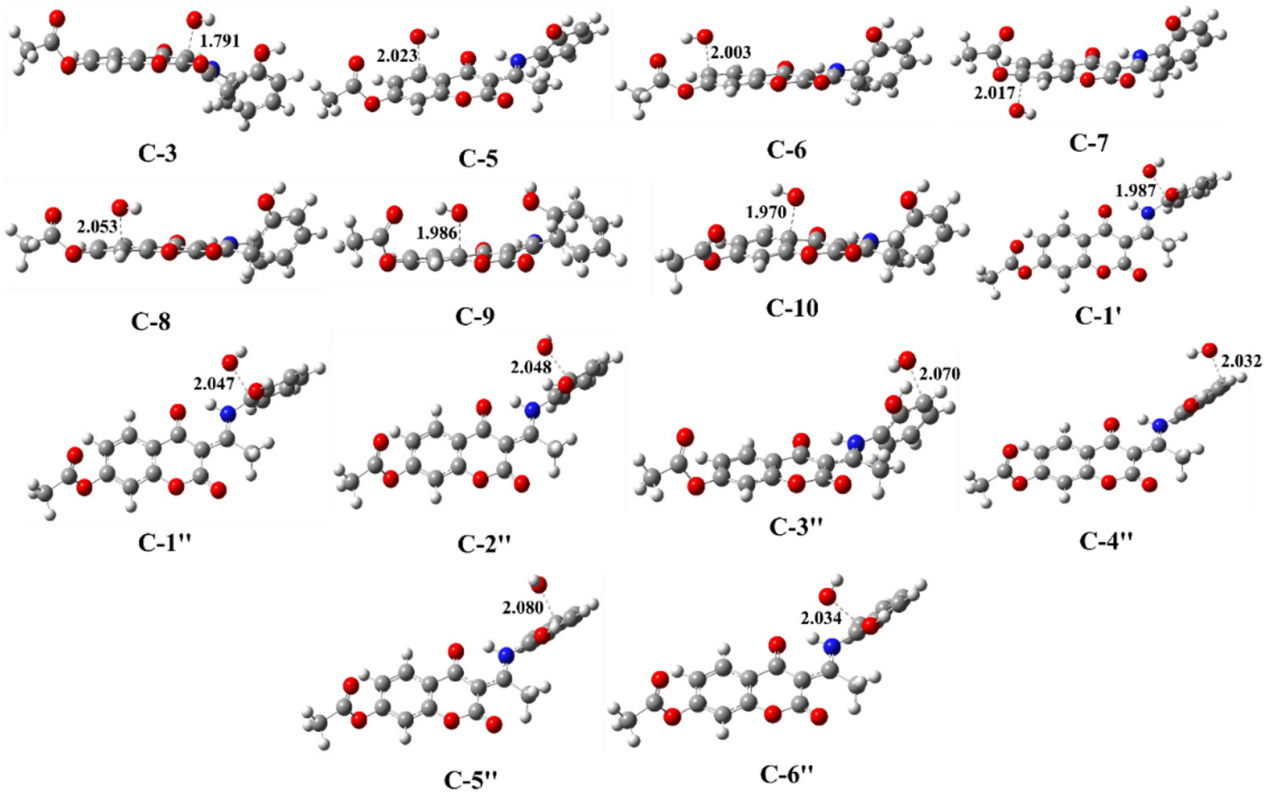

Figure 6. Optimized transition state geometries for radical adduct formation for A_2–RH and HO$^\bullet$ in water at M06-2X/6−311++G(d,p) level of theory.

Analogously to the HAT/PCET mechanism, the geometries of the transition states for the proton transfer reactions (SPL mechanism) have not been found, despite numerous attempts. In this case, the dependence of the total energy (a.u.) on the distance was monitored. The constant decrease in energy indicated that these reactions occurred without an activation barrier as diffusion-controlled processes (Figure S7, 1.91×10^9 $M^{-1}{\cdot}s^{-1}$) [52–54]. The electron transfer rate constants estimated using Marcus theory decreased in this sequence: A_1–RH (8.02×10^9 $M^{-1}{\cdot}s^{-1}$) > A_2–RH (8.01×10^9 $M^{-1}{\cdot}s^{-1}$) > A_3–RH (7.90×10^9 $M^{-1}{\cdot}s^{-1}$). Based on these results, the formation of $A_1-R^\bullet$ was a kinetically favored process, while $A_3-R^\bullet$ was thermodynamically preferred (Tables 2 and 3). The stability of $A_2-R^\bullet$ depended on the position of the OH substituent and the delocalization of unpaired electrons through the structure. No additional hydrogen bonds were observed.

Table 3. Estimated values of reaction Gibbs energies ($\Delta_r G$) in $kJ{\cdot}mol^{-1}$ for reactions between the biologically important target molecules and the formed $A_1-R^\bullet$, $A_2-R^\bullet$, $A_3-R^\bullet$ radicals at 298.15 K.

Target Molecule	A_1–$O^\bullet$	A_2–$O^\bullet$	A_3–$O^\bullet$	$HO^\bullet$
LM	62	65	63	−190
NF−Leu (γ−site)	−16	−13	−15	−111
NF−Cys (SH site)	18	21	19	−145
NF−Tyr (OH site)	9	12	10	−136
NF−Tyr (SET)	139	148	155	127
NF−Trp (SET)	92	101	108	80
NF−Met (γ−site)	−13	−10	−12	−114
NF−His (SET)	−5	−2	−3	−123
G	17	14	16	−110
2dG	30	27	29	−97

Using the individual rate constants, the overall rate constant ($k_{overall}$) was determined as a measure of the susceptibility of a compound to the AOPs involving $HO^\bullet$ (Table S2). All investigated compounds showed a high overall rate constant, with a negligible decrease in activity in the following order: A_1–RH (1.21×10^{10} $M^{-1}{\cdot}s^{-1}$) > A_2–RH (1.19×10^{10} $M^{-1}{\cdot}s^{-1}$) > A_3–RH (1.18×10^{10} $M^{-1}{\cdot}s^{-1}$). This correlated well with the experimental values obtained with EPR spectroscopy. This comparison proved the applicability of the QM-ORSA methodology for the prediction of the capacity and mechanisms of the radical action of the investigated compounds.

To evaluate the relative amounts of products, as well as the influence of individual reaction pathways on the overall capacity, branching ratios (Γ_i, %) were estimated (Table S2). The results in Table S2 indicate that HAT and SPLET were the dominant mechanisms in the $HO^\bullet$ removal process. Radicals in the HAT/PCET mechanism and anionic species in the SPL mechanism were formed in significant percentages: 16.06% (A_1–RH), 15.78% (A_2–RH), and 16.20% (A_3–RH). Radicals formed during the electron transfer from the phenoxide anions to $HO^\bullet$ were present in the highest relative percentages: 67.40% (A_1–RH), 66.16% (A_2–RH), and 67.00% (A_3–RH). The difference in the stabilization of anions and radicals overcame the importance of the substitution position in the cases of A_2–RH and A_3–RH, thus leading to the higher experimental and theoretical reactivity of the former towards $HO^\bullet$.

Finally, based on the $k_{overall}$ value, it was possible to estimate the half-life ($\tau_{1/2}$) values of the investigated compounds exposed to $HO^\bullet$ radicals. The $\tau_{1/2}$ values calculated under physiological conditions and with different concentrations of $HO^\bullet$ are presented in Table S3. In natural water, $[HO^\bullet]_{aq}$ concentrations ranged from 10^{-18} or 10^{-14} M to ca. 10^{-10} M in the AOP system. Specifically, at very low concentrations of $HO^\bullet$ in the range from approximately 10^{-18} to 10^{-16} M, the $\tau_{1/2}$ for degradation of A_1–RH−A_3–RH was in the range of 679.9–6.6 days. At $HO^\bullet$ concentrations between 10^{-15} and 10^{-14} M, the $\tau_{1/2}$ decreased to 16.8–1.6 h. At the $HO^\bullet$ concentration of 10^{-10} M, the half−life dropped

to ~0.6 s. Thus, the effectiveness of AOP technology was demonstrated, as well as the importance of theoretical investigations and modeling of these processes.

3.5. Damage to a Target Biomolecule

To obtain information about the reactivity of the formed radical species (A_1–$O^\bullet$, A_2–$O^\bullet$, and A_3–$O^\bullet$), interactions with the constituents of essential macromolecules—the phospholipid bilayer, proteins, and nucleic acids—were examined (Table 3). The optimized geometries of the reaction participants, neutral molecular targets, and corresponding radicals/radical cations are shown in Figure S8 and Figure 7. As expected, highly reactive radical species, such as $HO^\bullet$, interacted spontaneously with all investigated biomolecules (the lipid model (−190 kJ·mol^{-1}), amino acid residues (<−111 kJ·mol^{-1}), and nucleotides (<−97 kJ·mol^{-1})) except for NF-Trp (80 kJ·mol^{-1}).

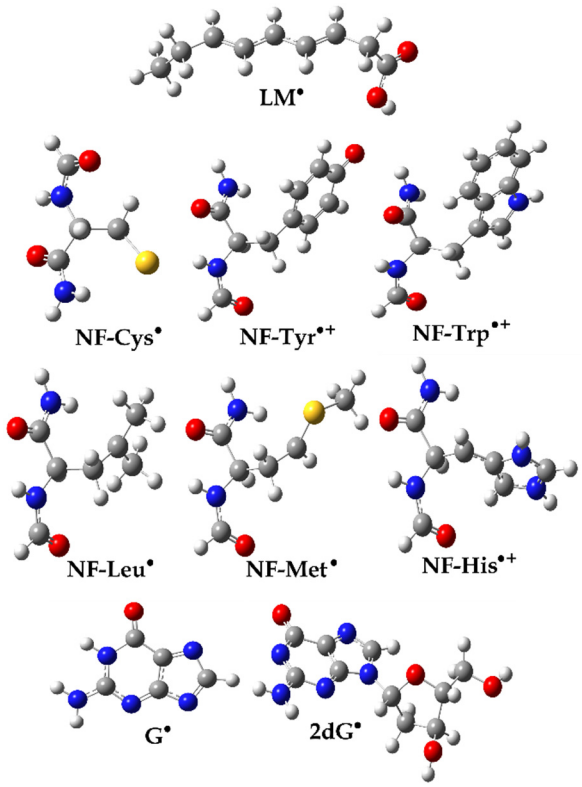

Figure 7. Optimized geometries of selected radicals/radical cations of biomolecular target compounds in water at M06-2X/6-311++G(d,p) level of theory.

The lipid model (**LM**) is a model of linoleic acid that was employed on the basis of literature data [55]. This unsaturated fatty acid has two allylic H atoms that can react with radical species through the HAT mechanism [56]. Endergonic reactions between the formed radicals and **LM** (>62 kJ·mol^{-1}) indicated that they do lead to the destruction of the building blocks of the cell membrane of living organisms.

Model compounds were chosen to represent the building blocks of proteins; amino acids have been successfully applied as reactive centers in the study of protein reactions [57]. Available literature data indicate that the selected amino acid residues (leucine (Leu), cysteine (Cys), methionine (Met), tyrosine (Tyr), histidine (His), and tryptophan (Trp)) are susceptible to radical attack [58]. These amino acid residues react with radical species through different mechanisms: SET (Tyr, Trp) and HAT (Cis, Leu, Met, His) [41]. Except for slightly exergonic $\Delta_r G$ values with the amino acid residues NF-Leu (γ-site) (<−13 kJ·mol^{-1}), NF-Met (γ-site) (<−10 kJ·mol^{-1}), and NF-His (γ-site) (–2 kJ·mol^{-1}), the newly formed radicals did not interact with the other investigated building blocks of the protein.

2′-Deoxyguanosine (2dG) and guanine (G), which is the most easily oxidized of all nucleobases, were chosen for oxidative DNA damage modeling [41,59]. The newly formed radical species did not interact with the building blocks of DNA molecules (nucleotides (>30 kJ·mol^{-1})), nor with the corresponding bases (>14 kJ·mol^{-1}), as indicated by the endergonic $\Delta_r G$ values.

3.6. Termination of A_n–R• Reactions by Synergistic Reactions with O_2/NO and HO•

Although the formed radicals did not show activity towards important constituents of biomolecules, the question of their further fate remained open. Based on available literature data [38], two possible reaction paths comprising radical inactivation and the formation of neutral products were proposed. For A_n–R• radical species, two carbon atoms located near the oxygen were chosen, and the hydrogen atom/proton abstraction process was modeled. The proposed reaction schemes for the mechanisms are presented in Figure 8, while the corresponding values of the thermodynamic parameters are summarized in Table 4.

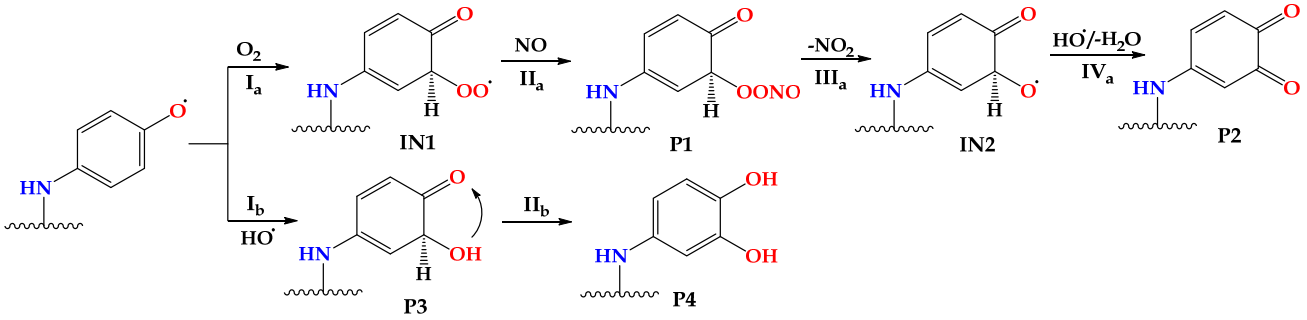

Figure 8. The proposed mechanism for the reaction between the formed radical species: A_n–R• and O_2/NO (Ia, IIa, IIIa, IVa) and A_n–R• and HO• (Ib, IIb).

Table 4. Estimated values of reaction Gibbs energies ($\Delta_r G$) in kJ·mol^{-1} for reactions between the formed radicals A_1−R•, A_2−R•, and A_3−R• and O_2/NO in different sequential reaction pathways (I_a, II_a, III_a, IV_a) or HO• (I_b, II_b) at 298.15 K.

Radical	Position	I_a	II_a	III_a	IV_a	I_b	II_b
A_1–O•	C-3	−98	−32	−15	−416	−207	−101
	C-5	−112	−28	−10	−421	−207	/
A_2–O•	C−2	−110	−21	−29	−419	−211	−107
	C-4	−116	−21	−24	−414	−214	−107
A_3–O•	C-3	−95	−31	−9	−438	−200	−116
	C-5	−98	−28	−27	−421	−211	−111

Available literature data indicate the ability of radicals to react synergistically with O_2/NO and form neutral products (Figures 8 and 9, P2) [38]. A variable concentration of dissolved molecular oxygen (O_2) in water enables the reaction with radical species leading to the formation of a corresponding peroxide adduct (IN1, Ia, Figure S9), which can further react with the NO present in natural and wastewater to form a radical adduct (P1, IIa, Figure S10). The next step involved the spontaneous intramolecular separation of NO_2 molecules (IIIa) with the formation of the intermediate radical adduct IN2 (Figure S11). In this specific context, $\Delta_r G$ was exergonic and thermodynamically favored, especially in the case of the addition of molecular oxygen (Table 4). Finally, the action of HO•, through a highly exergonic mechanism (<−414 kJ·mol^{-1}) that has already been observed in our previous research, was found to result in the intramolecular separation of water molecules (IVa) and the formation of a neutral product (P2, Figure 9).

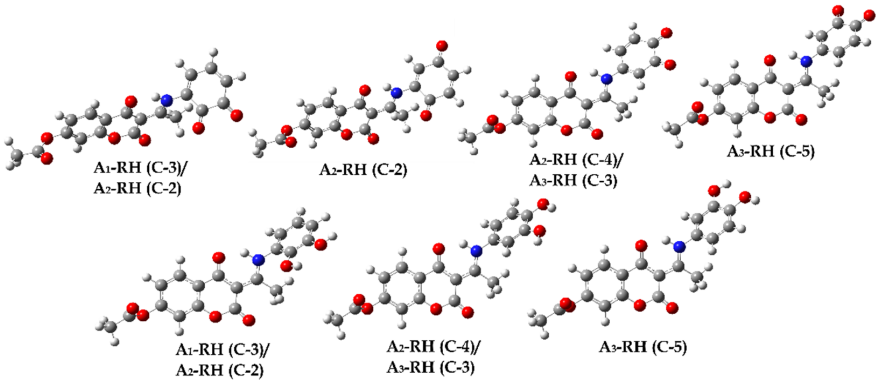

Figure 9. Optimized geometries of neutral final products P2 (**top**) and P4 (**bottom**) in water at M06−2X/6−311++G(d,p) level of theory.

Another mechanism has also been postulated and discussed in detail in previous work focused on AOP systems [24,24,53]. It involves the reaction of a formed radical with another $HO^{\bullet}$ radical (Ib), resulting in the formation of a neutral product (P3, Figure S12). In the next step, through keto–enol tautomerism (IIb) in a highly exergonic process (>−101 $kJ \cdot mol^{-1}$, Table 2), a catechol-type product is formed (P4).

3.7. Ecotoxicological Approach

The resulting stable oxidation products (P2, P4) were subjected to acute and chronic ecotoxicity estimation investigations for aquatic organisms: fish, daphnia, and green algae. The results, obtained as part of the ECOSAR program, together with the reference values published by the European Union (acute toxicity, described in Annex VI of Directive 67/548/EEC) [60] and in the Chinese hazard evaluation guidelines for new chemical substances (chronic toxicity, HJ/T 154-2004) [61], are summarized in Table 5.

Table 5. Estimated ecotoxicity values of A_1–RH, A_2–RH, and A_3–RH and their oxidation products in relation to aquatic organisms ($mg \cdot L^{-1}$) at pH = 7.4.

Products	Acute Toxicity *			Chronic Toxicity *		
	Fish LC_{50}	Daphnia LC_{50}	Green Algae EC_{50}	Fish ChV	Daphnia ChV	Green Algae ChV
A_1–RH	9.40	17.20	6.04	0.60	8.31	2.29
P1-C3/C5	27.40	3.54	2.49	1.24	0.32	0.88
P2-C3	99.6	11.60	10.1	6.28	0.93	3.28
P2-C5	59.1	7.40	5.73	3.30	0.60	1.92
P3-C3	49.8	6.10	4.77	2.67	0.51	1.61
P3-C5	199.00	22.00	21.20	14.80	1.67	6.65
P4-C3	18.7	36.10	13.70	1.21	20.30	4.43
A_2–RH	15.10	28.60	10.60	0.95	15.30	3.60
P1-C2/C4	86.70	10.30	8.58	5.15	0.84	2.83
P2-C2/C4	99.60	11.60	10.10	6.28	0.93	3.28
P3-C2/C4	157.00	17.60	16.40	11.10	1.37	5.22
P4-C2	18.70	36.10	13.70	1.21	20.30	4.43
P4-C4	30.00	60.00	24.10	2.10	36.90	6.69
A_3–RH	15.10	28.60	10.60	0.95	15.30	3.60
P1-C3/C5	86.70	10.30	8.58	5.15	0.84	2.83
P2-C3/C5	99.6	11.60	10.10	6.28	0.93	3.28
P3-C3/C5	157.00	17.60	16.40	11.10	1.37	5.22
P4-C3/C5	30.00	60.00	24.10	2.10	36.90	6.69

* Reference values [60,61]. Not harmful: log LC_{50} > 100 or log EC_{50} > 100. Log ChV > 10. Harmful: 10 < log LC_{50} < 100 or 10 < log EC_{50} < 100. 1 < log ChV < 10. Toxic: 1 < log LC_{50} < 10 or 1 < log EC_{50} < 10. 0.1 < log ChV < 1. Very toxic: log LC_{50} < 1 or log EC_{50} < 1. Log ChV < −0.1.

All starting compounds (A_1–RH, A_2–RH, and A_3–RH) showed harmful acute (<15.10 mg·L^{-1}) and chronic toxic effects (<1 mg·L^{-1}) on fish. On the other hand, all oxidation products showed less acute harmful (>18.70 mg·L^{-1}) and chronic (>1.21 mg·L^{-1}) toxicity. In contrast, the oxidative product P3 of all compounds was entirely harmless in terms of acute (>157.00 mg·L^{-1}) and chronic toxicity (>11.10 mg·L^{-1}). In general, oxidation product P4 showed a less acute harmful effect on daphnia (>36.10 mg·L^{-1}) in comparison to neutral compounds, while being utterly harmless in terms of chronic toxicity (>20.30 mg·L^{-1}). Oxidation products P3 and P4 showed fewer harmful effects in terms of acute (>13.10 mg·L^{-1}) and chronic toxicity (>4.43 mg·L^{-1}) in comparison to the neutral starting compounds. A similar trend was observed in the interpretation of the ecotoxicological status of green algae.

4. Conclusions

Application of advanced oxidation processes to stable coumarin derivatives is one way to remove them from wastewater and decrease the toxicity towards aquatic organisms. Three aminophenol derivatives of 4,7–hydroxycoumarin and $HO^\bullet$ were employed for experimental and theoretical examination of the relevant reaction mechanisms. Based on the results of EPR measurements, it can be concluded that the investigated compounds showed high reactivity towards the $HO^\bullet$ radical, with a decrease in reactivity in the following order A_1–RH (91%) > A_2–RH (88%) > A_3–RH (81%). At the physiological pH value, all three compounds presented as neutral species (>99%), followed by the monoanionic forms. Analysis of the thermodynamic and kinetic parameters confirmed that the hydrogen atom transfer (HAT), sequential proton loss followed by electron transfer (SPLET), and radical adduct formation (RAF) mechanisms were the operative reaction pathways in the degradation of the studied compounds induced by the $HO^\bullet$ radical. The hydrogen atom and electron transfers represented diffusion-controlled reactions, while the RAF rate constants were between 10^3 and 10^7 $M^{-1}s^{-1}$, depending on the reaction site. Estimated overall rate constants ($k_{overall}$) decreased slightly in the order: A_1–RH (1.21×10^{10} $M^{-1}{\cdot}s^{-1}$) > A_2–RH (1.19×10^{10} $M^{-1}{\cdot}s^{-1}$) > A_3–RH (1.18×10^{10} $M^{-1}{\cdot}s^{-1}$), as obtained using the QM−ORSA methodology, showing excellent agreement with the reactivity order observed using EPR spectroscopy. The anionic species present greatly influenced the overall rate constant, leading to the obtained order of reactivity. The stability of the formed radical and anionic species resulted from extended delocalization and weak interactions between groups within compounds. The estimated values of the branching ratios (Γ_i, %) of products indicated that the degradation of the investigated compounds induced by $HO^\bullet$ mainly occurred via HAT and SPLET mechanisms, with half-life ($\tau_{1/2}$) values of ca. 0.6 s. The distinctly endergonic $\Delta_r G$ values for the reaction of the formed radicals ($A_1-R^\bullet$, $A_2-R^\bullet$, and $A_3-R^\bullet$) and the biomolecule building blocks (linoleic acid, amino acids, and guanine) demonstrated the importance of the lower toxicity of products in AOPs. As expected, the $\Delta_r G$ values were more endergonic compared to the interaction of the $HO^\bullet$ radical and the investigated macromolecular targets. The formed radical species could further interact with the O_2/NO and $HO^\bullet$ present in wastewaters to end the cycle and form neutral species. The thermodynamic favorability of these reaction pathways was reflected in the highly exergonic $\Delta_r G$ values for the four/two steps of the proposed mechanisms The formed neutral products had lower acute and chronic toxicity than the starting neutral compounds, as estimated in the ECOSAR program, towards daphnia, fish, and green algae. The presented experimental/theoretical results demonstrate the applicability of the proposed mechanisms. They open the way for future analysis and application of the mentioned theoretical approach in developing advanced oxidation processes and highlight the need for reliable determination of toxicity towards aquatic organisms.

Supplementary Materials: The following are available online at https://www.mdpi.com/article/10.3390/ijerph20032046/s1, Figure S1: Optimized geometries of radical adducts formed between A_1–RH and HO$^\bullet$ at M06-2X/6-311++G(d,p) level of theory with characteristic bond distances (Å); Figure S2: Optimized geometries of radical adducts formed between A_2–RH and HO$^\bullet$ at M06-2X/6-311++G(d,p) level of theory with characteristic bond distances (Å); Figure S3: Optimized geometries of radical adducts formed between A_3–RH and HO$^\bullet$ at M06-2X/6-311++G(d,p) level of theory with characteristic bond distances (Å); Table S1. Estimated values of kinetic parameters: activation energy (ΔG_a, kJ·mol^{-1}) and rate constants of the bimolecular chemical reactions (M^{-1}·s^{-1}) between the investigated compounds A_1–RH, A_2–RH, and A_3–RH and HO$^\bullet$ estimated using conventional transition state theory (k_{TST}); Figure S4: Dependence of total energy (a.u.) on the characteristic HO–H2 (A_1–RH, top), HO–H3 (A_2–RH, center), and HO–H4 (A_3–RH, bottom) distances (Å) for the HAT/PCET mechanism; Figure S5: Optimized transition state geometries for the formation of radical adducts between A_2–RH and HO$^\bullet$ in water at M06-2X/6-311++G(d,p) level of theory; Figure S6: Optimized transition state geometries for the formation of radical adducts between A_3–RH and HO$^\bullet$ in water at M06-2X/6-311++G(d,p) level of theory; Figure S7: Dependence of total energy (a.u.) on the characteristic HO–H2 (A_1–RH, top), HO–H3 (A_2–RH, center), and HO–H4 (A_3–RH, bottom) distances (Å) for the SPL mechanism; Table S2. Estimated overall rate constants ($k_{overall}$) and branching ratios (Γ_i, %) at pH = 7.4 for newly synthesized coumarin derivatives A_1–RH–A_3–RH; Table S3. Half−lives ($\tau_{1/2}$) of investigated compounds (A_1–RH–A_3–RH) at physiological pH (7.4) and different concentrations (M) of HO$^\bullet$ radicals; Figure S8: Optimized geometries of the selected biomolecular target compound in water at M06-2X/6-311++G(d,p) level of theory; Figure S9. Optimized geometries of intermediate radical adducts (IN1) formed in the reactions between A_1–RH (top), A_2–RH (center), and A_3–RH (bottom) and O_2 in water at M06-2X/6-311++G(d,p) level of theory; Figure S10. Optimized geometries of intermediate adducts (P1) formed in the reactions between A_1–R$^\bullet$ (IN1, top), A_2–R$^\bullet$ (IN1, center), and A_3–R$^\bullet$ (IN1, bottom) and NO in water at M06-2X/6-311++G(d,p) level of theory; Figure S11. Optimized geometries of intermediate radical adducts (IN2) formed in the intramolecular separation of NO_2 molecules in A_1–R$^\bullet$ (P1, top), A_2–R$^\bullet$ (P1, center), and A_3–R$^\bullet$ (P1, bottom) in water at M06-2X/6-311++G(d,p) level of theory; Figure S12. Optimized geometries of intermediate adducts (P3) formed in the reactions between A_1–R$^\bullet$ (top), A_2–R$^\bullet$ (center), and A_3–R$^\bullet$ (bottom) and HO$^\bullet$ in water at M06-2X/6-311++G(d,p) level of theory.

Author Contributions: All authors contributed substantially to the work. Conceptualization, E.A., Z.M., Ž.M. and R.V.; methodology, Ž.M., D.D., E.K. and D.B.; investigation, Ž.M., D.D., D.B., M.Ž., Z.M., E.A., E.K., J.D.M., V.L. and M.B.; resources, Z.M., D.D., M.Ž. and M.B.; formal analysis, E.A., Z.M., J.D.M. and V.L.; writing—original draft preparation, D.B., Ž.M. and R.V.; writing—review and editing, Ž.M., D.D., D.B., M.Ž., Z.M., E.A. and V.L.; visualization, Ž.M.; project administration, Z.M. and D.D. All authors have read and agreed to the published version of the manuscript.

Funding: This work was supported by the Serbian Ministry of Education, Science, and Technological Development (agreement nos 451-03-68/2022-14/200122, 451-03-68/2022-14/200378, and 451-03-68/2022-14/200053).

Institutional Review Board Statement: Not applicable.

Informed Consent Statement: Not applicable.

Data Availability Statement: Data are contained within the article and Supplementary Materials.

Conflicts of Interest: The authors declare no conflict of interest.

References

1. Zhang, L.; Xu, Z. Coumarin-containing hybrids and their anticancer activities. *Eur. J. Med. Chem.* **2019**, *181*, 111587. [CrossRef] [PubMed]
2. Thakur, A.; Singla, R.; Jaitak, V. Coumarins as anticancer agents: A review on synthetic strategies, mechanism of action and SAR studies. *Eur. J. Med. Chem.* **2015**, *101*, 476–495. [CrossRef]
3. Ojala, T.; Remes, S.; Haansuu, P.; Vuorela, H.; Hiltunen, R.; Haahtela, K.; Vuorela, P. Antimicrobial activity of some coumarin containing herbal plants growing in Finland. *J. Ethnopharmacol.* **2000**, *73*, 299–305. [CrossRef] [PubMed]
4. Al-Majedy, Y.K.; Kadhum, A.A.H.; Al-Amiery, A.A.; Mohamad, A.B. Coumarins: The antimicrobial agents. *Sys. Rev. Pharm.* **2017**, *8*, 62. [CrossRef]

5. Fylaktakidou, K.C.; Hadjipavlou-Litina, D.J.; Litinas, K.E.; Nicolaides, D.N. Natural and synthetic coumarin derivatives with anti-inflammatory/antioxidant activities. *Curr. Pharm. Des.* **2004**, *10*, 3813–3833. [CrossRef] [PubMed]
6. Al-Majedy, Y.; Al-Amiery, A.; Kadhum, A.A.; BakarMohamad, A. Antioxidant activity of coumarins. *Sys. Rev. Pharm.* **2017**, *8*, 24. [CrossRef]
7. Mishra, S.; Pandey, A.; Manvati, S. Coumarin: An emerging antiviral agent. *Heliyon* **2020**, *6*, e03217. [CrossRef]
8. Hu, Y.; Chen, W.; Shen, Y.; Zhu, B.; Wang, G.X. Synthesis and antiviral activity of coumarin derivatives against infectious hematopoietic necrosis virus. *Bioorg. Med. Chem. Lett.* **2019**, *29*, 1749–1755. [CrossRef]
9. Lei, L.; Xue, Y.B.; Liu, Z.; Peng, S.S.; He, Y.; Zhang, Y.; Fang, R.; Wang, J.P.; Luo, Z.W.; Yao, G.M.; et al. Coumarin derivatives from Ainsliaea fragrans and their anticoagulant activity. *Sci. Rep.* **2015**, *5*, 13544. [CrossRef]
10. Arora, R.B.; Mathur, C.N. Relationship between structure and anticoagulant activity of coumarin derivatives. *Br. J. Pharmacol.* **1963**, *20*, 29–35.
11. Yates, R.A.; Wong, J.; Seiberling, M.; Merz, M.; März, W.; Nauck, M. The effect of anastrozole on the single-dose pharmacokinetics and anticoagulant activity of warfarin in healthy volunteers. *Br. J. Clin. Pharmacol.* **2001**, *51*, 429–435. [CrossRef] [PubMed]
12. Kataranovski, M.; Kataranovski, D.; Zolotarevski, L.; Jović, M. Epicutaneous exposure to anticoagulant rodenticide warfarin modulates local skin activity in rats. *Cutan. Ocul. Toxicol.* **2007**, *26*, 1–13. [CrossRef] [PubMed]
13. Gómez-Canela, C.; Barata, C.; Lacorte, S. Occurrence, elimination, and risk of anticoagulant rodenticides and drugs during wastewater treatment. *Environ. Sci. Pollut. Res.* **2014**, *21*, 7194–7203. [CrossRef] [PubMed]
14. Popp, D.; Plugge, C.M.; Kleinsteuber, S.; Harms, H.; Sträuber, H. Inhibitory effect of coumarin on syntrophic fatty acid-oxidizing and methanogenic cultures and biogas reactor microbiomes. *Appl. Environ. Microbiol.* **2017**, *83*, e00438-17. [CrossRef]
15. Guerra-Rodríguez, S.; Rodríguez, E.; Singh, D.N.; Rodríguez-Chueca, J. Assessment of sulfate radical-based advanced oxidation processes for water and wastewater treatment: A review. *Water* **2018**, *10*, 1828. [CrossRef]
16. Amor, C.; Marchão, L.; Lucas, M.S.; Peres, J.A. Application of advanced oxidation processes for the treatment of recalcitrant agro-industrial wastewater: A review. *Water* **2019**, *11*, 205. [CrossRef]
17. Garrido-Cardenas, J.A.; Esteban-García, B.; Agüera, A.; Sánchez-Pérez, J.A. Manzano-Agugliaro, F.; Wastewater treatment by advanced oxidation process and their worldwide research trends. *Int. J. Environ. Res. Public Health* **2020**, *17*, 170. [CrossRef]
18. Deng, Y.; Zhao, R. Advanced oxidation processes (AOPs) in wastewater treatment. *Curr. Pollut. Rep.* **2017**, *1*, 167–176. [CrossRef]
19. Pignatello, J.J.; Oliveros, E.; MacKay, A. Advanced oxidation processes for organic contaminant destruction based on the Fenton reaction and related chemistry. *Crit. Rev. Environ. Sci.* **2006**, *36*, 1–84. [CrossRef]
20. Chaplin, B.P. Critical review of electrochemical advanced oxidation processes for water treatment applications. *Environ. Sci. Process. Impacts.* **2014**, *16*, 1182–1203. [CrossRef]
21. Milanović, Ž.B.; Marković, Z.S.; Dimić, D.S.; Klisurić, O.R.; Radojević, I.D.; Šeklić, D.S.; Avdović, E.H.; Živanović, M.N.; Marković, J.D.; Radulović, M. Synthesis, structural characterization, biological activity and molecular docking study of 4, 7-dihydroxycoumarin modified by aminophenol derivatives. *C. R. Chim.* **2021**, *24*, 215–232. [CrossRef]
22. Galano, A.; Alvarez-Idaboy, J.R. A computational methodology for accurate predictions of rate constants in solution: Application to the assessment of primary antioxidant activity. *J. Comput. Chem.* **2013**, *34*, 2430–2445. [CrossRef] [PubMed]
23. Dimić, D.S.; Milenković, D.A.; Avdović, E.H.; Nakarada, Đ.J.; Marković, J.M.D.; Marković, Z.S. Advanced oxidation processes of coumarins by hydroperoxyl radical: An experimental and theoretical study, and ecotoxicology assessment. *Chem. Eng. J.* **2021**, *424*, 130331. [CrossRef]
24. Dimić, D.; Milanović, Ž.; Jovanović, G.; Sretenović, D.; Milenković, D.; Marković, Z.; Marković, J.D. Comparative antiradical activity and molecular Docking/Dynamics analysis of octopamine and norepinephrine: The role of OH groups. *Comput. Biol. Chem.* **2020**, *84*, 107170. [CrossRef]
25. Milanović, Ž.; Dimić, D.; Žižić, M.; Milenković, D.; Marković, Z.; Avdović, E. Mechanism of Antiradical Activity of Newly Synthesized 4, 7-Dihydroxycoumarin Derivatives-Experimental and Kinetic DFT Study. *Int. J. Mol. Sci.* **2021**, *22*, 13273. [CrossRef]
26. Amić, A.; Dimitrić Marković, J.M.; Marković, Z.; Milenković, D.; Milanović, Ž.; Antonijević, M.; Mastiľák Cagardová, D.; Rodríguez-Guerra Pedregal, J. Theoretical Study of Radical Inactivation, LOX Inhibition, and Iron Chelation: The Role of Ferulic Acid in Skin Protection against UVA Induced Oxidative Stress. *Antioxidants* **2021**, *10*, 1303. [CrossRef] [PubMed]
27. Jackson, S.K.; Liu, K.J.; Liu, M.; Timmins, G.S. Detection and removal of contaminating hydroxylamines from the spin trap DEPMPO, and re-evaluation of its use to indicate nitrone radical cation formation and SN1 reactions. *Free Radic. Biol. Med.* **2002**, *32*, 228–232. [CrossRef]
28. Frisch, M.J.; Trucks, G.W.; Schlegel, H.B.; Scuseria, G.W.; Robb, M.A.; Cheeseman, J.R.; Scalmani, G.; Barone, V.; Mennucci, B.; Petersson, G.A.; et al. *Gaussian 09*; Gaussian, Inc.: Wallingford, CT, USA, 2009.
29. Becke, A.D.; Johnson, E.R. A density-functional model of the dispersion interaction. *J. Chem. Phys.* **2005**, *123*, 154101. [CrossRef]
30. Antonijević, M.R.; Avdović, E.H.; Simijonović, D.M.; Milanović, Ž.B.; Amić, A.D.; Marković, Z.S. Radical scavenging activity and pharmacokinetic properties of coumarin–hydroxybenzohydrazide hybrids. *Int. J. Mol. Sci.* **2022**, *23*, 490. [CrossRef]
31. Milenković, D.A.; Dimić, D.S.; Avdović, E.H.; Amić, A.D.; Marković, J.M.D. Marković, Z.S.; Advanced oxidation process of coumarins by hydroxyl radical: Towards the new mechanism leading to less toxic products. *Chem. Eng. J.* **2020**, *395*, 124971. [CrossRef]
32. Takano, Y.; Houk, K.N. Benchmarking the conductor-like polarizable continuum model (CPCM) for aqueous solvation free energies of neutral and ionic organic molecules. *J. Chem. Theory Comput.* **2005**, *1*, 70–77. [CrossRef] [PubMed]

33. Pechukas, P. Transition state theory. *Annu. Rev. Phys. Chem.* **1981**, *32*, 159–177. [CrossRef]
34. Dhali, R.; John, C.; Swathi, R.S. Quantum Transmission of He Isotopes through Crown Ether-Embedded Graphene Nanomeshes: An Eckart Potential Approach. *J. Phys. Chem. A* **2019**, *123*, 7499–7506. [CrossRef] [PubMed]
35. Miller, W.H. Tunneling corrections to unimolecular rate constants, with application to formaldehyde. *J. Am. Chem. Soc.* **1979**, *101*, 6810–6814. [CrossRef]
36. Duncan, W.T.; Bell, R.L.; Truong, T.N. TheRate: Program for ab initio direct dynamics calculations of thermal and vibrational-state-selected rate constants. *J. Comput. Chem.* **1998**, *19*, 1039–1052. [CrossRef]
37. Reuschenbach, P.; Silvani, M.; Dammann, M.; Warnecke, D.; Knacker, T. ECOSAR model performance with a large test set of industrial chemicals. *Chemosphere* **2008**, *71*, 1986–1995. [CrossRef]
38. An, Z.; Sun, J.; Han, D.; Mei, Q.; Wei, B.; Wang, X.; He, M. Theoretical study on the mechanisms, kinetics and ecotoxicity assessment of OH-initiated reactions of guaiacol in atmosphere and wastewater. *Sci. Total Environ.* **2019**, *685*, 729–740. [CrossRef]
39. Spielmann, H. White Paper of the Commission of European Community–strategy for a future chemicals policy. *Altex* **2001**, *18*, 147–148.
40. Von Gunten, U.; Oliveras, Y. Kinetics of the reaction between hydrogen peroxide and hypobromous acid: Implication on water treatment and natural systems. *Water Res.* **1997**, *31*, 900–906. [CrossRef]
41. Castañeda-Arriaga, R.; Pérez-González, A.; Reina, M.; Alvarez-Idaboy, J.R.; Galano, A. Comprehensive investigation of the antioxidant and pro-oxidant effects of phenolic compounds: A double-edged sword in the context of oxidative stress? *J. Phys. Chem. B* **2018**, *122*, 6198–6214. [CrossRef]
42. Avdović, E.H.; Dimić, D.S.; Marković, J.M.D.; Vuković, N.; Radulović, M.Đ.; Živanović, M.N.; Filipović, N.; Đorović, J.; Trifunović, S.; Marković, Z.S. Spectroscopic and theoretical investigation of the potential anti-tumor and antimicrobial agent, 3-(1-((2-hydroxyphenyl) amino) ethylidene) chroman-2, 4-dione. *Spectrochim. Acta A Mol.* **2019**, *206*, 421–429. [CrossRef] [PubMed]
43. Avdović, E.H.; Stojković, D.L.; Jevtić, V.V.; Kosić, M.; Ristić, B.; Harhaji-Trajković, L.; Vukić, M.; Vuković, N.; Marković, Z.; Potočňák, I.; et al. Synthesis, characterization and cytotoxicity of a new palladium (II) complex with a coumarin-derived ligand 3-(1-(3-hydroxypropylamino) ethylidene) chroman-2, 4-dione. Crystal structure of the 3-(1-(3-hydroxypropylamino) ethylidene)-chroman-2, 4-dione. *Inorg. Chim. Acta* **2017**, *466*, 188–196. [CrossRef]
44. Avdović, E.H.; Milanović, Ž.B.; Molčanov, K.; Roca, S.; Vikić-Topić, D.; Mrkalić, E.M.; Jelić, R.; Marković, Z.S. Synthesis, characterization and investigating the binding mechanism of novel coumarin derivatives with human serum albumin: Spectroscopic and computational approach. *J. Mol. Struct.* **2022**, *1254*, 132366. [CrossRef]
45. Galano, A. On the direct scavenging activity of melatonin towards hydroxyl and a series of peroxyl radicals. *Phys. Chem. Chem. Phys.* **2011**, *15*, 7178–7188. [CrossRef] [PubMed]
46. Galano, A.; Alvarez-Idaboy, J.R. Kinetics of radical-molecule reactions in aqueous solution: A benchmark study of the performance of density functional methods. *J. Comput. Chem.* **2014**, *28*, 2019–2026. [CrossRef] [PubMed]
47. Wang, J.L.; Xu, L.J. Advanced oxidation processes for wastewater treatment: Formation of hydroxyl radical and application. *Crit. Rev. Environ. Sci.* **2012**, *45*, 251–325. [CrossRef]
48. Cheng, M.; Zeng, G.; Huang, D.; Lai, C.; Xu, P.; Zhang, C.; Liu, Y. Hydroxyl radicals based advanced oxidation processes (AOPs) for remediation of soils contaminated with organic compounds: A review. *Chem. Eng. J.* **2016**, *284*, 582–598. [CrossRef]
49. Tai, C.; Peng, J.F.; Liu, J.F.; Jiang, G.B.; Zou, H. Determination of hydroxyl radicals in advanced oxidation processes with dimethyl sulfoxide trapping and liquid chromatography. *Anal. Chim. Acta* **2004**, *527*, 73–80. [CrossRef]
50. Liu, Y.; He, X.; Fu, Y.; Dionysiou, D.D. Degradation kinetics and mechanism of oxytetracycline by hydroxyl radical-based advanced oxidation processes. *Chem. Eng. J.* **2016**, *284*, 1317–1327. [CrossRef]
51. ACD/Percepta. ACD/Labs Release 2020.2.0. Available online: https://www.acdlabs.com/products/percepta/predictors/pka/ (accessed on 1 December 2022).
52. Milanović, Ž.; Tošović, J.; Marković, S.; Marković, Z. Comparison of the scavenging capacities of phloroglucinol and 2, 4, 6-trihydroxypyridine towards HO radical: A computational study. *RSC Adv.* **2020**, *10*, 43262–43272. [CrossRef]
53. Milanović, Ž.; Dimić, D.; Antonijević, M.; Žižić, M.; Milenković, D.; Avdović, E.; Marković, Z. Influence of acid-base equilibria on the rate of the chemical reaction in the Advanced Oxidation Processes: Coumarin derivatives and hydroxyl radical. *Chem. Eng. J.* **2023**, *453*, 139648. [CrossRef]
54. Tošović, J.; Marković, S. Antioxidative activity of chlorogenic acid relative to trolox in aqueous solution–DFT study. *Food Chem.* **2019**, *278*, 469–475. [CrossRef]
55. Castañeda-Arriaga, R.; Galano, A. Exploring Chemical Routes Relevant to the Toxicity of Paracetamol and Its meta-Analogue at a Molecular Level. *Chem. Res. Toxicol.* **2017**, *30*, 1286–1301. [CrossRef]
56. Reid, D.L.; Armstrong, D.A.; Rauk, A.; Von Sonntag, C. H-atom abstraction by thiyl radicals from peptides and cyclic dipeptides. A theoretical study of reaction rates. *Phys. Chem. Chem. Phys.* **2003**, *5*, 3994–3999. [CrossRef]
57. Moosmann, B.; Behl, C. Cytoprotective antioxidant function of tyrosine and tryptophan residues in transmembrane proteins. *Eur. J. Biochem.* **2000**, *267*, 5687–5692. [CrossRef] [PubMed]
58. Domazou, A.S.; Koppenol, W.H.; Gebicki, J.M. Efficient repair of protein radicals by ascorbate. *Free Radical Biol. Med.* **2009**, *46*, 1049–1057. [CrossRef]

59. Seidel, C.A.M.; Schulz, A.; Sauer, M.H.M. Nucleobase-Specific Quenching of Fluorescent Dyes. 1. Nucleobase One-Electron Redox Potentials and Their Correlation with Static and Dynamic Quenching Efficiencies. *J. Phys. Chem.* **1996**, *100*, 5541–5553. [CrossRef]
60. Directive, C. Council Directive 67/548/EEC of 27 June 1967 on the approximation of laws, regulations and administrative provisions relating to the classification, packaging and labelling of dangerous substances. *Off. J. Eur. Communities* **1967**, *196*, 1.
61. Lau, M.H.Y.; Leung, K.M.Y.; Wong, S.W.Y.; Wang, H.; Yan, Z.G. Environmental policy, legislation and management of persistent organic pollutants (POPs) in China. *Environ. Pollut.* **2012**, *165*, 182–192. [CrossRef] [PubMed]